Indentation Analysis of Linear-Chain Hydrocarbon Monolayers Anchored to Diamond

Alan B. Tutein,[†] **Steven J. Stuart,**[‡] **and Judith A. Harrison*,†**

*Department of Chemistry, United States Naval Academy, Annapolis, Maryland 21402,
and Department of Chemistry, Clemson University, Clemson, South Carolina 29634*

Classical molecular dynamics simulations are used to examine the indentation of monolayers composed of linear hydrocarbon chains with 8, 13, or 22 carbon atoms that are chemically bound (or anchored) to a diamond (111) substrate. Indentation is accomplished using both a flexible and rigid single-wall, capped [10,10] nanotube as the tip. Regardless of the nanotube used, the simulations show that indentation of the hydrocarbon monolayers causes a disruption of the original ordering of the monolayer, pinning of selected hydrocarbon chains beneath the tube, and the formation of gauche defects within the monolayer. Because nanotubes are stiff along their axial direction, the flexible nanotube is distorted only slightly by its interaction with the softer monolayers. However, interaction with the hard diamond substrate causes the tube to buckle. Severe indents with a rigid nanotube tip result in rupture of chemical bonds within the hydrocarbon monolayer.

Introduction

Technological applications, such as microelectromechanical systems[1,2] and magnetic storage devices,[3−5] have piqued interest in the potential use of organic films for boundary-layer lubricants. In these applications, the thickness of the lubricating films is approaching the monolayer regime. At these thicknesses, adhesion of the molecules to the substrate is of paramount importance, particularly in applications that involve the relative motion of solid surfaces in contact. In addition, the lubricant monolayers must possess the desired friction and wear properties. Thus, monolayers formed from self-assembly that are covalently bonded to the substrate, such alkanethiols and alkylsilanes, are better candidates for boundary-layer lubricants than Langmuir-Blodgett (LB) films. As a result, the molecular structure, mechanical properties, and tribological properties of self-assembled monolayer (SAM) materials have been studied a great deal using scanning probe microscopies.[6−14]

The aforementioned experimental examinations of SAM systems have revealed several interesting phenomena. Salmeron and co-workers examined C_{18} *n*-alkanethiols on Au using an atomic force microscope (AFM).[7] Imaging the alkanethiol monolayer at low load yielded images that had the periodicity of the thiol layers observed in other AFM experiments (($\sqrt{3} \times \sqrt{3}$) *R* 30°).[12,13] As pressure increased, the AFM images of the thiol lattice became increasingly disordered. At a well-defined critical pressure the (1 × 1) periodicity of the Au(111) substrate was observed. Reducing the pressure and imaging resulted in the reappearance of the thiol lattice.

A number of groups have examined the friction and wear properties of alkanethiols on Au and alkylsilane monolayers on both Si and mica using AFM.[6,8,11,14] Short-chain alkanethiols, less than ∼8 carbon atoms, are less densely packed than longer chains and thus have more defects. For both types of monolayers, these studies have shown that the friction decreased

as the length of the alkyl portion of the chain increased. Adhesion between the AFM tip and the monolayer decreased as the chain length increased,[6] presumably due to the decreased contact area that arises from the decreased compressibility of the films. This trend in adhesive forces has also been observed in Langmuir-Blodgett (LB) films.[15]

Motivated by the aforementioned experimental studies and the recent interest in monolayer lubricants, this work utilizes molecular dynamics (MD) simulations to examine monolayers of *n*-alkanes that are chemically bound or anchored to diamond substrates. A single-wall, capped armchair nanotube is used to examine the atomic-scale events that occur during indentation of the hydrocarbon monolayers. The effects of tip flexibility, length of the monolayer chain, and indentation speed on the indentation process are all examined. Particular attention will be paid to the formation of defects, monolayer mechanical response, and bond rupture (and formation) during the course of tip indentation and extraction. Previous MD simulations have examined the structure[16−19] and compression of *n*-alkanethiols on Au.[20,21] The major difference between those studies and this work is that *irreversible* chemical changes (or changes in hybridization associated with bond rupture and formation) are possible in the studies presented here. In addition, this is the first computational study to systematically examine the effects of chain length on system properties. Subsequent studies will examine the dependence of friction on chain length.[22]

Methods and Procedures

All of the simulation systems contain a monolayer of hydrocarbon chains chemically bound (or anchored) to the (111) face of a diamond substrate (Figure 1a). Each layer of the diamond substrate contains 480 carbon atoms and the substrates normally contain 11 layers. Attached to the (111) face (top layer in Figure 1a) of the diamond substrate are saturated hydrocarbon chains: CH_3 -$(CH_2)_{n−1}$, with *n* = 8, 13, and 22 (referred to as C_8, C_{13}, and C_{22} monolayers, respectively). The computational cell in the plane that contains the monolayers is approximately 50.8 Å by 52.8 Å (or 22.4 Å² /monomer). A total of 120 hydrocarbon chains, with all of the dihedral angles of the carbon

* To whom correspondence should be addressed. Tel: 410-293-6624. Fax: 410-293-2218. E-mail: jah@nadn.navy.mil.
† United States Naval Academy.
‡ Clemson University.
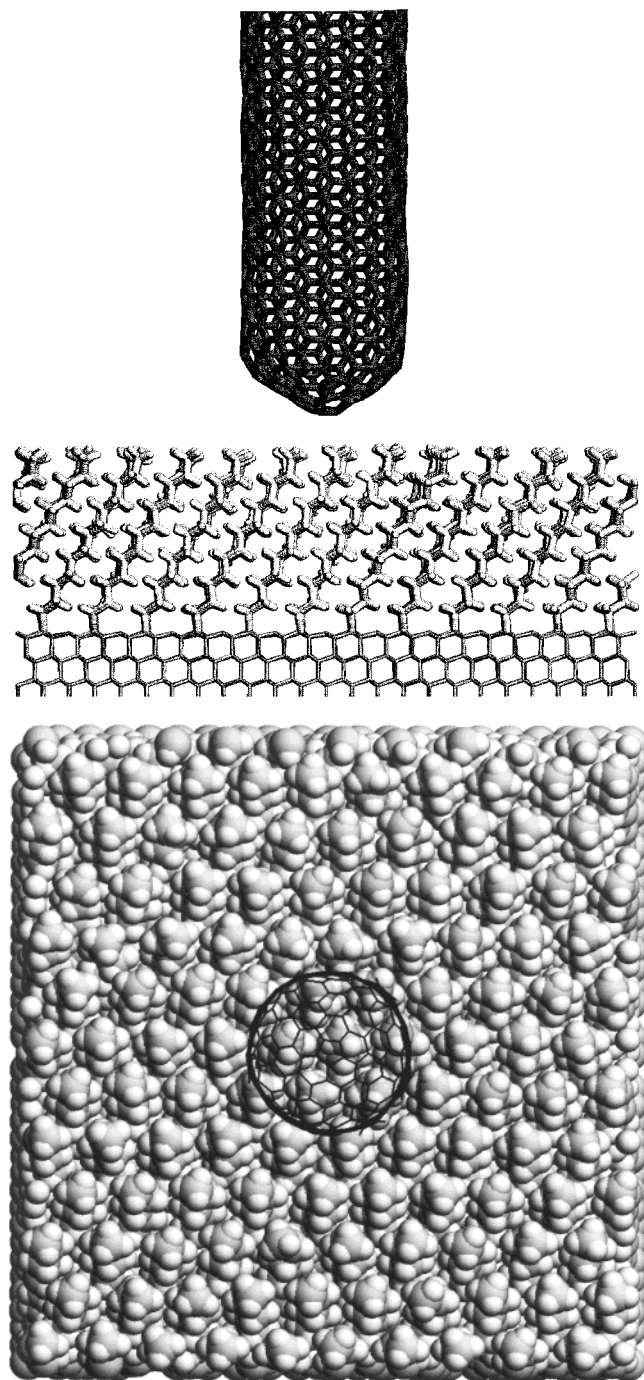
Figure 1. Snapshot of a sample starting configuration for the MD simulations. In (a) a single-wall, capped [10,10] carbon nanotube is shown in dark gray. Below the nanotube is a diamond substrate with a hydrocarbon monolayer attached to its (111) surface (both shown in light gray). Each chain of this monolayer is a saturated hydrocarbon containing 13 carbon atoms. The chains are in the anti conformation and are attached to the diamond in a (2×2) arrangement. The system is viewed along the [110] direction. In (b) the system is viewed along the [111] direction.

backbones in their anti configuration, are attached in a (2×2) arrangement to the diamond substrate (Figure 1b). This arrangement of chains was selected because it yields approximately the same packing density and *cant* as monolayers of alkanethiols on Au (111).[6]

A nanotube was selected as the probe (or tip) in part because Smalley and co-workers proposed that carbon nanotubes might constitute well-defined tips for scanning probe microscopies.[23]

In addition, the properties of flexible nanotubes have been studied previously by a number of groups using the reactive empirical bond-order (REBO) potential.[24–27] For instance, the suitability of capped nanotubes as scanning probe microscope (SPM) tips was first investigated using computer simulations by Harrison et al.[24] Yakobson et al. simulated the morphology and stress–strain curves of uncapped nanotubes.[25] The nanotube used for all indentations discussed here is a single-wall, [10,-10] nanotube capped with a C_{5v} hemifullerene dome. (For a more detailed explanation of the cap structure see Harrison et al.[24]) It contains 870 carbon atoms and has a diameter of approximately 14 Å and a length from base to the end of the cap of approximately 53 Å. The carbon atoms at the open end of the tube are hydrogen-terminated to satisfy the valence requirements of carbon. The number of atoms used to simulate the C_8, C_{13}, and C_{22} monolayers plus the diamond substrate are 9240, 11 040, and 11 400, respectively.

Prior to indentation, each monolayer system is allowed to equilibrate for a sufficient time to allow all energies and temperatures to reach their steady-state values. Simulations are performed by holding the bottom two layers of the diamond substrate rigid (Figure 1a). Moving upward from the bottom, the next two layers of the diamond are maintained at a constant temperature of 300 K using generalized Langevin dynamics to simulate coupling with an external heat bath.[28] The remaining diamond layers and the hydrocarbon chains are free to move according to classical dynamics. The equations of motion for all nonrigid atoms are integrated using the velocity Verlet algorithm with a constant step size of 0.25 fs.[29] Periodic boundary conditions are used in the plane of the surface to simulate an infinite interface.

The potential governing atomic motions is the recently developed adaptive intermolecular reactive empirical bond order (AIREBO) potential.[30] This variation of the Brenner REBO potential[31,32] introduces nonbonded interactions while preserving the chemical reactivity of the original REBO potential. Almost all of the covalent bonding parameters of the REBO potential have been preserved due to their success when applied to problems ranging from the initial stages of diamond growth[33] to the tribochemistry that occurs when chemically modified diamond surfaces are in sliding contact.[34,35]

The first enhancement to the REBO potential adds long-range or intermolecular interactions by introducing a Lennard-Jones 12-6 potential. The second enhancement is the inclusion of torsional interactions. A novel adaptive algorithm allows for the inclusion of these two enhancements for nonbonded interactions without compromising the unique ability of the REBO potential to model chemical reactions or changes in hybridization of the carbon atom. Thus, because chemical reactions are possible in these simulations, events such as interchain reactions and film rupture are possible.

Two separate sets of simulations are performed: one where the nanotube is flexible and one where the nanotube is kept rigid. The atoms in the flexible nanotube are partitioned in much the same way as the atoms in the substrate. The top two layers of atoms are rigid. Moving downward from the top, a Langevin thermostat, which is completely independent of the thermostat applied to the thermally controlled layers of the diamond, is applied to the next two layers of atoms, and the remaining layers act under no constraints whatsoever. In both cases, indentation is accomplished by moving all rigid atoms at a constant velocity toward the monolayer surface. Extraction of the nanotube is accomplished by reversing the direction of motion of the tube.

Indentation of Linear-Chain Hydrocarbon Monolayers

J. Phys. Chem. B, Vol. 103, No. 51, 1999 **11359**
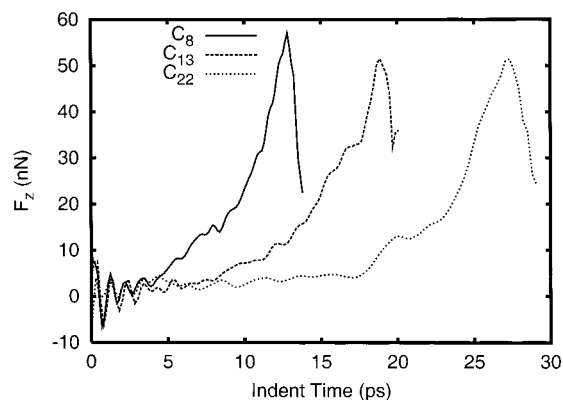
Figure 2. Load on the upper two layers of a *flexible* nanotube as a function of indentation time for the indentation of hydrocarbon monolayers. The solid, dashed, and dotted lines correspond to the C_8, C_{13}, and C_{22} monolayers, respectively. Other simulation conditions are given in the text.

The load on the probe tip is taken to be the total force on the rigid-layer atoms of the nanotube.

Unless otherwise indicated, all indentation (and extraction) velocities are 100 m/s. Limits on computation time constrain this indentation velocity to be many orders of magnitude greater that the 10^{-8} m/s speeds typically used in nanoindentation experiments[9,14] and still several orders of magnitude greater than the 10^{-1} m/s speeds commonly used in AFM tapping mode. Even at 100 m/s, there was adequate time for thermal equilibration of the simulation systems. In addition, simulations with indentation speeds of 50 m/s show qualitatively similar behavior for the majority of system properties, e.g., load on the tip. Thus, the simulations accurately describe most of the qualitative behavior that would be observed at much slower loading rates. However, some properties, such as the number of gauche defects formed during indentation, do depend strongly on the indentation speed.

Results

Load as a function of time for the indentation of the C_8, C_{13}, and C_{22} monolayers using a *flexible* [10,10] nanotube is shown in Figure 2. In all cases, the load fluctuates a small amount prior to surface contact, then it increases monotonically until a sharp discontinuity is reached. The small fluctuations in the load prior to tip contact are the result of longitudinal vibrations of the tip induced by the available thermal energy.[36] The discontinuity marks one of the distinct conformational changes the nanotube undergoes during indentation. Snapshots from the simulated indentation of the C_{13} monolayer are shown in Figure 3. As the nanotube comes into contact with the monolayer, the load on the tube increases. Interaction of the nanotube with the monolayer during indentation causes the nanotube to be deflected slightly from perpendicular or tilted (Figure 3a). Because the nanotube is tilted from its penetration into the monolayer, when it encounters the hard diamond substrate the force on the nanotube is sufficient to cause it to begin to buckle (Figure 3b). This stress-relieving deformation was also observed when the same type of nanotube was brought into contact with a hydrogen-terminated diamond substrate.[24] Once buckling occurs, the majority of the stress on the nanotube is relieved, which is apparent from the discontinuities at long times in Figure 2. Continued downward motion of the nanotube causes more deformation of the nanotube, not penetration into the diamond substrate (Figure 3c).

The majority of the changes imparted to the monolayers as a result of indentation depend little on the flexibility of the
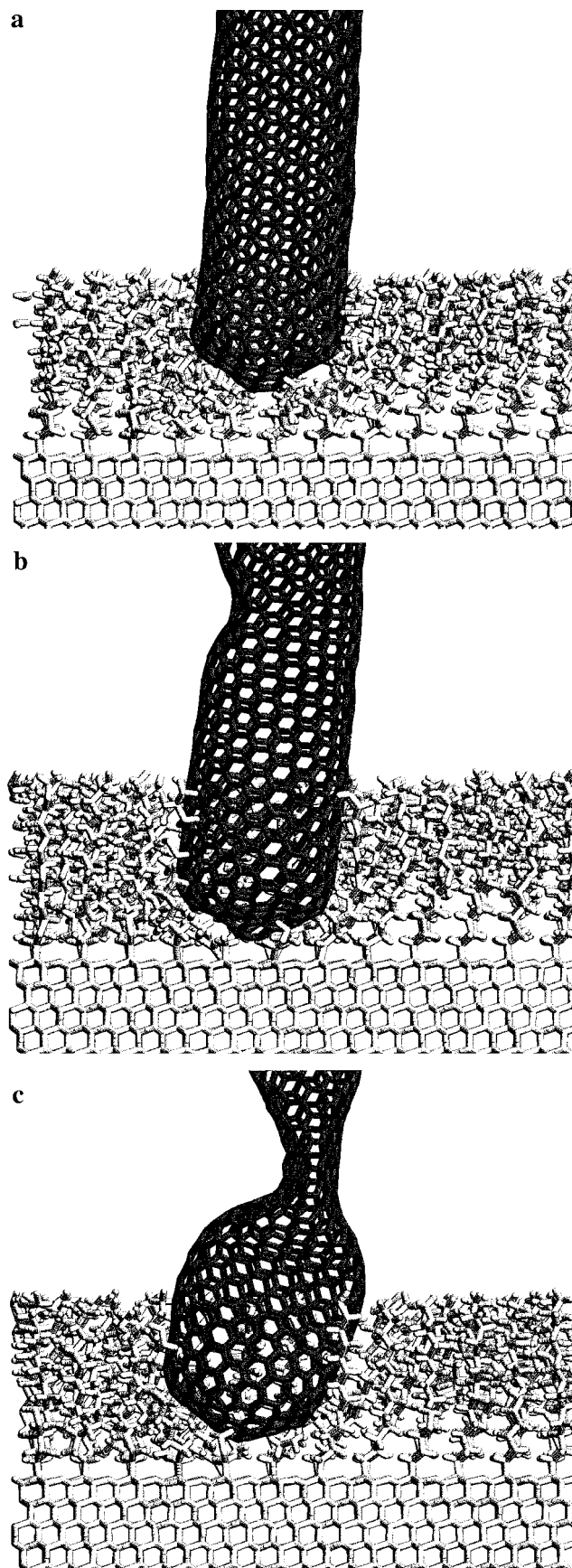
Figure 3. Snapshots from the MD simulations of the interaction of the *flexible*, capped [10,10] nanotube with a monolayer composed of C_{13} chains. The simulation times (load on the nanotube's rigid layers) are 13.5 ps (19.8 nN), 19.2 ps (41.2 nN), and 20.1 ps (36.0 nN) in (a), (b), and (c), respectively. Colors are the same as those used in Figure 1.
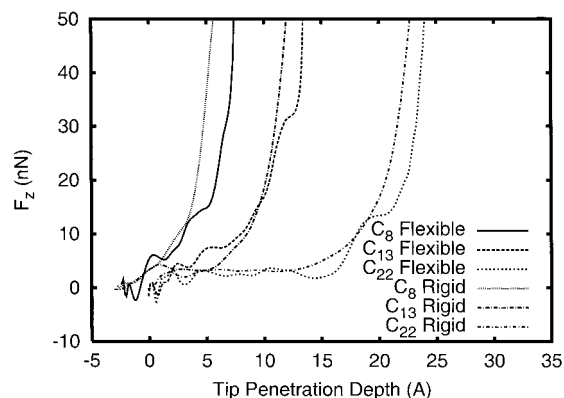
Figure 4. Load on the nanotube as a function of penetration depth for the indentation of C_8, C_{13}, and C_{22} hydrocarbon monolayers. Data for the indents using a *flexible* and a *rigid* nanotube tip are all shown.

nanotube. This is apparent from examination of force curves (Figure 4) obtained from indenting with a *flexible* and a *rigid* nanotube. For each system, these curves are qualitatively similar. Both types of nanotubes deform a small number of the chains within the monolayer during indentation (Figure 5a). (A C_{13} monolayer is shown in Figure 5. Similar behavior is observed when C_8 and C_{22} monolayers are indented with *rigid* nanotubes.) Eventually, these chains become "pinned" under the nanotube (Figure 5b). There are some notable differences that occur during indentation when a *rigid* nanotube is used, however. The *rigid* nanotube does not tilt as it penetrates the monolayer or buckle when it encounters the diamond substrate, and irreversible disruption of the monolayers occurs for extreme indentations. A single chain can become trapped directly under the nanotube. Continued indentation causes the chain to be squeezed against the hard diamond substrate. Eventually, an intrachain carbon— carbon bond ruptures (Figure 5c).

It should be noted that while the tilt induced in the *flexible* nanotube as a result of the indentation does not qualitatively affect the indentation process, it significantly affects the study of friction. Because the nanotube is tilted and embedded in the monolayer, movement of the tube parallel to the monolayer causes the tube to buckle and be lifted out of the monolayer.[37] Therefore, single-wall nanotubes may not be ideally suited for use as SPM probes in all instances, particularly if the aim of the experiment is to study tribological properties. With that in mind, the majority of our simulations were carried out with a *rigid* nanotube.

The pinning of selected hydrocarbon chains underneath the nanotube is also apparent in histograms of the *cant*, or tilt angle θ versus chain number (Figure 6). The tilt angle θ is the angle formed by the surface normal and the chain-axis vectors and is given by $\cos(\theta) = z/b$, where z is the length of a hydrocarbon chain along its carbon—carbon backbone and h is the height of the hydrocarbon chain above the diamond substrate. Prior to indentation and after equilibration, the values of θ for the C_{13} hydrocarbon chains are all tightly clustered about 32° (dashed line in Figure 6). This is similar to the experimentally determined cant of monolayers with similar packing densities.[6] Indentation of the C_{13} monolayer with the nanotube causes most of the chains to be "pushed" aside, decreasing their values of θ. That is, the majority of the hydrocarbon chains are "standing up" straighter (solid and dotted lines in Figure 6) due to the volume occluded by the nanotube. The chains with the very large θ values have been pinned under the nanotube. Defects introduced into the monolayer from interacting with the tip disrupt the order of the monolayer and may affect the monolayer's tribological
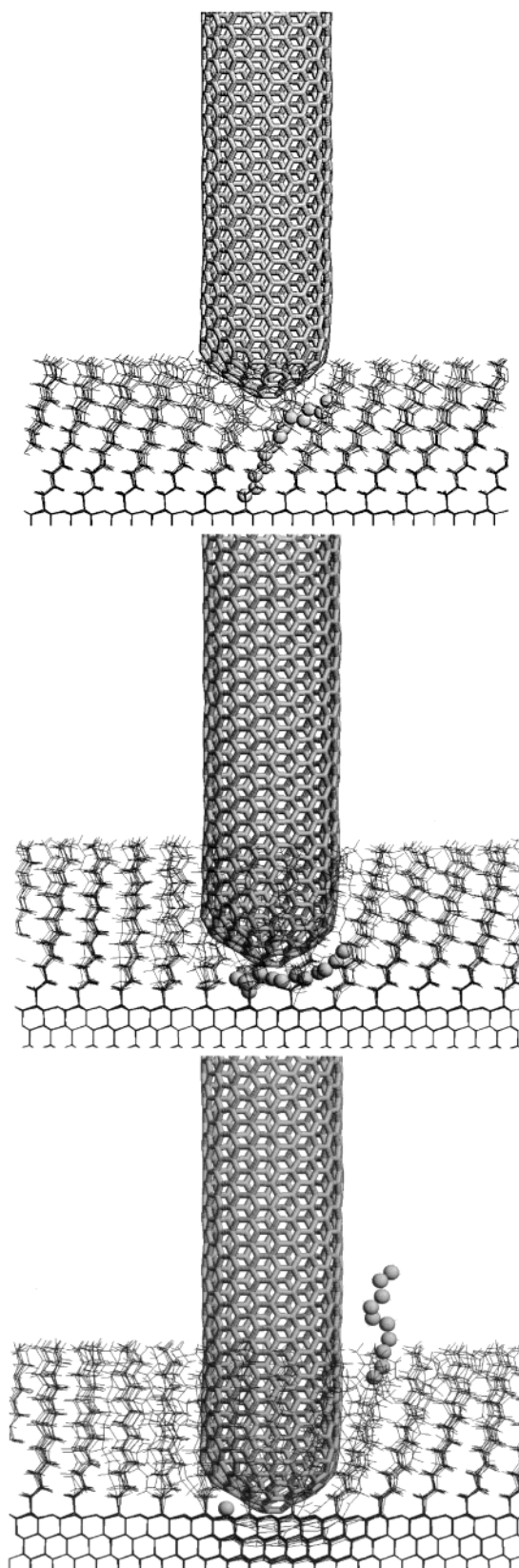

Figure 5. Snapshots from the MD simulations of the interaction of the *rigid*, capped [10,10] nanotube with a monolayer composed of C_{13} chains. The simulation times (load on the nanotube's rigid layers) are 24.0 ps (4.5 nN), 32.2 ps (38.9 nN), and 36.2 ps (239.9 nN) in (a), (b), and (c), respectively. The carbon atoms of one hydrocarbon chain that was significantly deformed (or pinned) and suffered a bond rupture are shown as gray spheres. For clarity, the remaining atoms in the substrate and monolayer are represented in a very thin wireframe format and the majority of the atoms in the diamond substrate are not shown. The nanotube is represented as it is in Figure 1.

Indentation of Linear-Chain Hydrocarbon Monolayers

J. Phys. Chem. B, Vol. 103, No. 51, 1999 **11361**
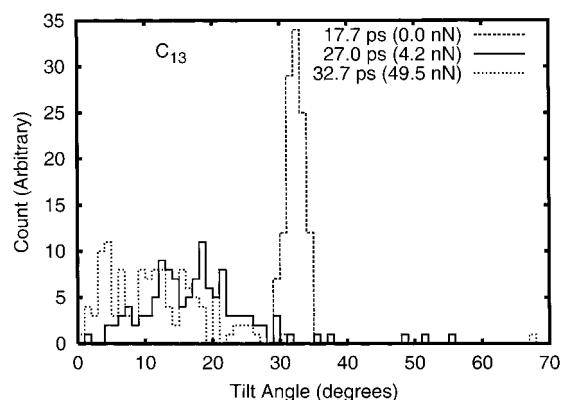

Figure 6. Histogram of tilt angles θ at various simulation times for the indentation of a C_{13} monolayer with a rigid nanotube.
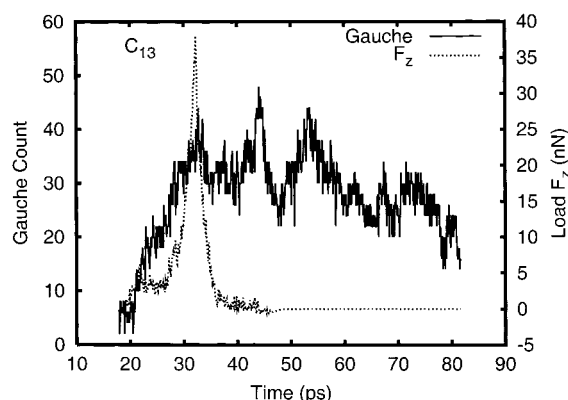

Figure 7. Number of gauche defects (solid line) within the monolayer and the load on the nanotube (dotted line) as a function of simulation time for the indentation (and extraction) of a rigid nanotube from a C_{13} monolayer.

properties. After equilibration at 300 K, the values of intrachain C−C−C−C dihedral-angle ϕ are all centered about ~180°, corresponding to the anti conformation. (This conformation has also been referred to as the *all trans* arrangement in the literature.[38]) It is clear from examination of Figure 7 that indentation causes the formation of *gauchelike* defects ($\phi > 270°$ or $\phi < 90°$) within the monolayer. Defects begin to form when the nanotube contacts the monolayer. Continued indentation results in a significant increase in the number of defects. These defects remain in the monolayer for some time after the external load is removed. Similar memory effects have been observed in SFA experiments.[39]

The shape of the nanotube is responsible for localizing the gauche defects to the region of the monolayer adjacent to and under the nanotube (Figure 8). The small radius of the nanotube allows it to "slice" into the monolayer, interacting with a small number of hydrocarbon chains. This causes the defects to be localized near the tip irrespective of the identity of the monolayer being indented. A second consequence of the small radius of the tip is that the number of defects formed depends on the depth of penetration into the monolayer rather than the length of the hydrocarbon chain (Figure 9). Thus, for a given penetration depth into the monolayer, all of the monolayer systems examined here have approximately the same number of gauche defects. It should also be noted that for a given penetration depth the load on the nanotube is the smallest for the monolayer composed of C_{22} chains and largest for the monolayer composed of C_8 chains (Figure 4). In other words, to achieve the same load, the monolayers composed of longer chain alkanes must be indented further. Thus, for a given load,
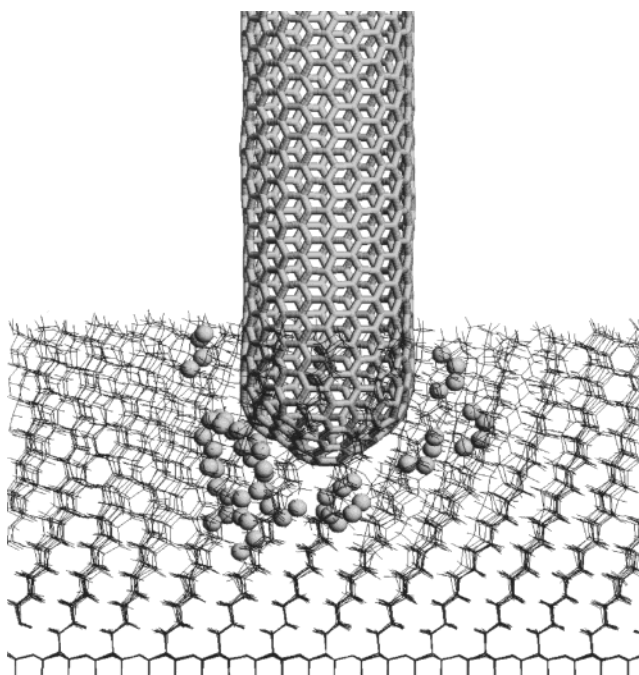
Figure 8. Snapshot from the MD simulation depicting the indentation of a *rigid*, capped [10,10] nanotube with a monolayer composed of C_{22} chains. Sets of carbon atoms within the monolayer chains whose dihedral angles are in their gauche conformation are represented as large gray spheres. For clarity, the remaining atoms in the substrate and monolayer are represented in a very thin wireframe format and the majority of the atoms in the diamond substrate are not shown. The nanotube is represented as it is in Figure 1.
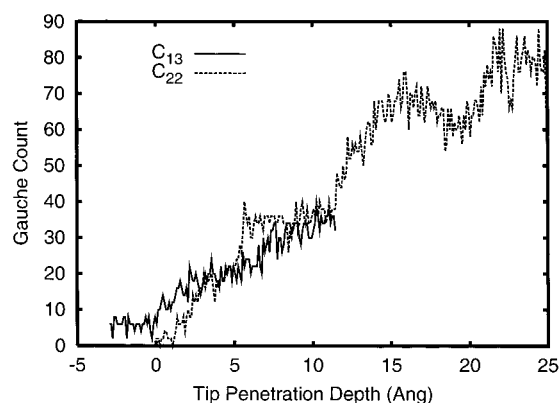
Figure 9. Number of gauche defects within the monolayer as a function of penetration depth for the indentation of a rigid nanotube into a C_{13} and a C_{22} monolayer at 100 m/s.
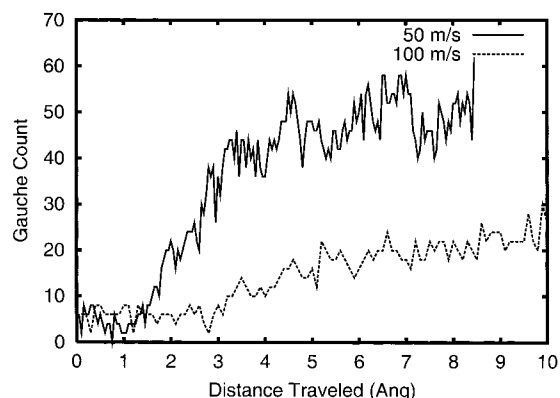
more defects will be present in the monolayer composed of C_{22} chains, fewer will be present in the C_{13} monolayer, and the fewest in the monolayer composed of C_8 chains.

The load on the nanotube as a function of penetration depth is independent of the indentation speed. However, the indentation speed has a profound effect on the number of gauche defects formed. Plots of the number of defects as a function of distance traveled by the nanotube (Figure 10) for two different indentation speeds (100 and 50 m/s) clearly show that slower indentation speeds lead to the formation of more defects.

The response of the monolayers to indentation can also be quantified by calculating a two-dimensional (2-D) structure factor, S_α. This quantity is given by

$$S_\alpha = \langle \cos \mathbf{k}_\alpha \cdot \mathbf{r}_{ij} \rangle \tag{1}$$

where the $\mathbf{k}_\alpha$ is a reciprocal lattice vector, and $\mathbf{r}_{ij} = \mathbf{r}_i - \mathbf{r}_j$ is

11362 *J. Phys. Chem. B, Vol. 103, No. 51, 1999*

Tutein et al.

Figure 10. Number of gauche defects within the monolayer as a function of distance traveled by the nanotube for the indentation of a *rigid* nanotube into a C_{13} monolayer at two different indentation speeds. The same starting configuration was used for each simulation.

the vector between atoms *i* and *j*. For a crystal with well-defined 2-D symmetry translations, the reciprocal lattice vectors $\mathbf{k}_\alpha$ can be calculated from the primitive lattice translations $\boldsymbol{\tau}_1$ and $\boldsymbol{\tau}_2$ using

$$\mathbf{k}_1 = 2\pi \frac{\boldsymbol{\tau}_1 - \alpha_2 \boldsymbol{\tau}_2}{\boldsymbol{\tau}_1 \cdot (\boldsymbol{\tau}_1 - \alpha_2 \boldsymbol{\tau}_2)} \tag{2}$$

and

$$\mathbf{k}_2 = 2\pi \frac{\boldsymbol{\tau}_2 - \alpha_1 \boldsymbol{\tau}_1}{\boldsymbol{\tau}_2 \cdot (\boldsymbol{\tau}_2 - \alpha_1 \boldsymbol{\tau}_1)} \tag{3}$$

where

$$\alpha_n = \frac{\boldsymbol{\tau}_1 \boldsymbol{\tau}_2}{\boldsymbol{\tau}_n \boldsymbol{\tau}_n} \tag{4}$$

These definitions guarantee that $\mathbf{k}_i \cdot \boldsymbol{\tau}_j = \delta_{ij} 2\pi$, as is true with the more familiar three-dimensional reciprocal lattice vectors. With these definitions, the 2-D structure factor S_α will have a value of one if the system is translationally invariant under $\boldsymbol{\tau}_1$ and $\boldsymbol{\tau}_2$. Consequently, individual $-CH_2-$ or $-CH_3$ segments of a well-ordered SAM will have S_α values near one if the reciprocal lattice vectors are calculated based on their 2×2 arrangement on the diamond substrate. The S_α values will decrease as the monolayer loses its translational order, averaging about zero for a completely disordered system.

The reciprocal lattice vectors appropriate for atoms in the (2×2) arrangement on a diamond (111) surface are used to compute the values of S_α shown in Figures 11 and 12. Figure 11 shows S_2 for the carbon atoms in the $-CH_2-$ (or CH_3) chain segments for equilibrated monolayers. For a given monolayer, the S_α values are closer to unity for segments closer to the diamond substrate. Thus, carbon atoms in the chain segments of the monolayer are more ordered the closer they are to the diamond attachment site, as expected. Comparison of segments the same distance from the diamond substrate but in different monolayers reveals that the longer chain monolayers are more ordered. Thus, the order in the films increases as the chain length increases. This trend is also observed in other monolayer systems that are bound to a substrate, such as alkylsilanes on mica.[40]

The S_α values for the indentation (and extraction) of a C_{13} monolayer with a *rigid* nanotube as a function of time are shown in Figure 12. Structure factors for all the segments within the
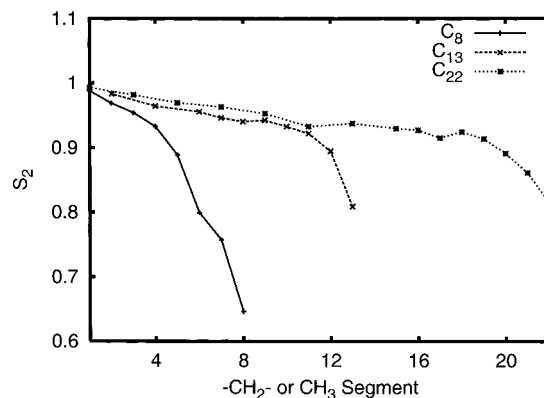

Figure 11. Two-dimensional structure factor S_2 as a function of chain segment ($-CH_2-$ or CH_3) for equilibrated C_8 (solid line), C_{13} (dashed line), and C_{22} (dotted line) monolayers. Error bars are approximately the size of the points.
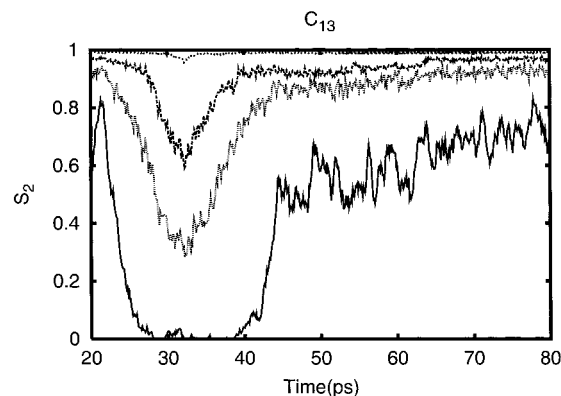
Figure 12. Two-dimensional structure factor S_2 as a function of simulation time for the indentation and extraction of a *rigid* nanotube with C_{13} monolayer. Small dotted, dashed, large dotted, and solid lines represent data from chain segments 1, 3, 5, and 13, respectively. Segment number 1 is attached to the diamond substrate. The motion of the tip is reversed at ~32 ps, and by ~45 ps the load on the tip is zero.

monolayer decrease due to the disruption of the translational order as the indentation proceeds. This is true regardless of the chain length of the monolayers. It should be noted that these monolayers are quite resilient. Except in the case of severe indents, retraction of the nanotube tip from the monolayer allows it to recover, given sufficient time, to an arrangement that is very close to its original lattice arrangement. That is, the S_α values are approaching their pre-indentation values. (This is also the case for the indentation of the C_8 and C_{22} monolayers.)

Load and displacement sensing techniques, such as nanoin-dentors and the AFM, provide information about a material's response to mechanical deformation.[41] In principle, mechanical property parameters such as Young's modulus and hardness can be extracted from these data. Because displacements recovered during unloading are largely elastic, elastic punch theory can be used to determine the modulus. Pharr et al. have shown that the initial *unloading* portion of a load-displacement curve is linear and the slope in this region is related to the reduced elastic modulus of the tip−sample system.[41] The load on the nanotube during indentation and extraction from a C_{13} monolayer is shown as a function of distance between the nanotube tip and the diamond substrate in Figure 13. This is for a fairly shallow indent so that the contributions from the diamond substrate are expected to be minimal. While there is some hysteresis in these data due to the formation of gauche defects, it is important to note that the initial slope of the unloading curve is approximately

Indentation of Linear-Chain Hydrocarbon Monolayers

J. Phys. Chem. B, Vol. 103, No. 51, 1999 **11363**
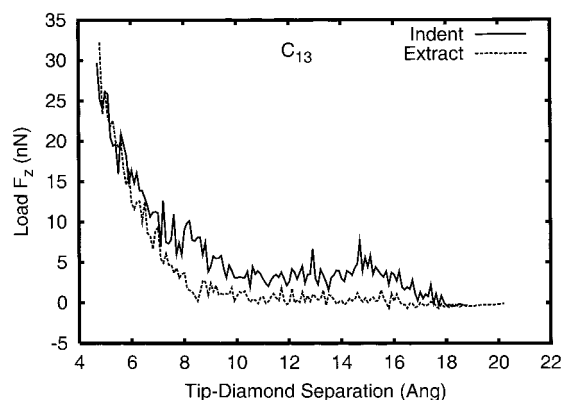
Figure 13. Load (force, F_z) on the nanotube as a function of separation of penetration depth. Indentation, or loading (solid line), and extraction, or unloading (dotted line), from a C_{13} monolayer are both shown.

Figure 14. Stress σ versus strain ϵ for the compression of hydrocarbon monolayers (C_8, C_{13}, and C_{22}) between rigid diamond surfaces. (Simulation details given in text.)

the same as the slope for the loading portion of the curve at similar separations. Thus, the slope of the loading curves can be used to obtain the reduced elastic modulus of the tip−sample system for these simulations. The load versus penetration is shown in Figure 4 for all the monolayer systems. Because the modulus of the tip is the same in each simulation, the difference in slopes apparent in Figure 4 is due to the response of the monolayers, with the C_{22} appearing softer than the C_{13} followed by the C_8.

Difficulties determining the contact area in AFM experiments make the quantitative determination of the Young's modulus of any sample from force-displacement data problematic. The modulus of chemically bound monolayer systems[6] (and in related systems[15,42]) has been inferred from pull-off force measurements made with the AFM. The adhesion of alkylsilanes on mica and alkanethiols on Au (111) show that adhesion is larger for monolayers composed of shorter chains. These adhesion measurements imply that the contact area is larger for the shorter chain molecules. Thus, one can infer that the modulus of the shorter chain molecules is lower. Related, nonchemically anchored, systems show similar trends in pull-off force. For instance, Koleske et al. examined mixed chain-length, phase-segregated Langmuir−Blodgett (LB) monolayers using atomic force microscopy.[15] Adhesion in the domains with 16 carbon atom chains (CH$_3$ (CH$_2$)$_{14}$ COOH or C_{16} for simplicity) was ∼20% higher than that in the domains composed of C_{24} chains. In all of these cases, the shorter chains appear to be more compliant. This conflicts with the trend observed here.

In an effort to resolve this apparent contradiction between theory and experiment, the elastic response of the monolayers in the indentation direction is examined using another approach. In a separate set of simulations, the nanotube is replaced with two layers of diamond and all but two layers of the diamond substrate holding the monolayers are removed. All the diamond layers are held rigid during the simulation, and the atoms within the monolayers are allowed to evolve in time without constraints. The monolayers are compressed by moving the upper diamond surface toward the monolayers at a constant velocity of 100 m/s.

The elastic constant c of an individual monolayer in the compression direction is given by $\sigma = c\epsilon$, where σ is the stress on the monolayer (force/area) and ϵ is the strain on the monolayer.[43,44] The strain is $(L - L_0)/L_0$, where L_0 is the average length of the chains in the compression direction prior to compression and L is the average length of the chains at a given time during the simulation. Plots of σ versus ϵ should be linear, with a slope that corresponds to the elastic constant in the compression direction.
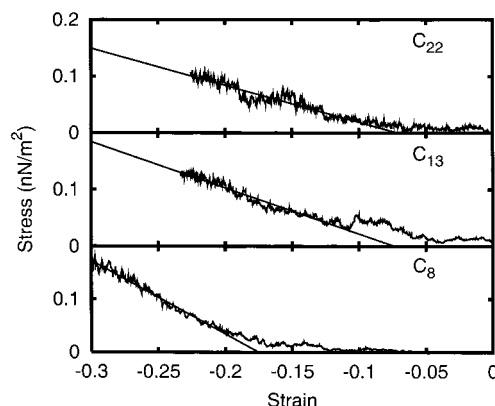
Stress is plotted as a function of strain for the C_8, C_{13}, and C_{22} monolayers in Figure 14. For all of the monolayers, these data are linear, and linear regression analysis yields values of 140 ± 1.0 GPa, 81 ± 0.9 GPa, and 65 ± 1.0 GPa for the elastic constants of the C_8, C_{13}, and C_{22} monolayers, respectively. Thus, the elastic constant in the compression direction (which is the same as the indentation direction) decreases as the chain length of the monolayer increases.

Using analytic functional forms for the tip shape it is possible to extract a Young's modulus from force-displacement data by using continuum mechanics theories. A Johnson-Kendall-Roberts fit to interfacial force microscope force-displacement indentation data of a C_{12} alkanethiol monolayer on Au yields an effective Young's modulus of 8 ± 1 GPa.[45] The value of 81 ± 0.9 GPa calculated here differs considerably. It is unclear what is responsible for the difference, although the presence of defects and domain boundaries in the experimental systems will likely result in lower moduli than for ideal monolayers.[6,46]

Discussion

The Young's modulus of the tubular region of carbon nanotubes has been shown to be approximately the same as the in-plane modulus of graphite or higher.[24,25,47−49] These simulations confirm that *flexible* capped nanotubes can be used to indent a variety of softer substrates, including monolayers composed of hydrocarbon chains. Analysis of animated sequences of the simulations shows the interaction of the nanotube with the monolayers causes the tip of the nanotube to be "tilted" slightly to the side (Figure 3a). Comparison of indentations using *flexible* and *rigid* nanotubes reveals that this tilting has little qualitative effect on the indentation. However, because nanotubes are fairly easy to bend in the transverse direction,[23,25] this deformation reduces the amount of additional force needed to buckle the nanotube. Thus, movement of the nanotube parallel to the monolayer, as would be needed to examine friction, causes the nanotube to bend. Therefore, these simulations indicate that the use of single-wall nanotubes to study tribological properties may be problematic. Because the Euler buckling force depends on the length of the nanotube, it may be possible to use very short nanotubes to examine tribological phenomena. However, this remains to be experimentally verified.

The order within hydrocarbon monolayers was determined by calculating the S_α values for carbon atoms in the −CH$_2$− (or CH$_3$) chain segments within a given monolayer. The larger S_α values per chain segment for the longer chain hydrocarbons show that at room temperature the longer hydrocarbon chains are more ordered (Figure 7). A similar trend is observed

experimentally for alkanethiols on Au.[38,40,50] In addition, the tilt angle of monolayer chains (~32°) is reasonable on the basis of experimentally determined cant of monolayers with similar packing densities.[6] Thus, it seems that modifications made to the potential energy function used here allow for the accurate modeling of hydrocarbon monolayer structures.[30]

Because the nanotubes reduce the volume available to the monolayer, the majority of the chains experience an increase in tilt angle θ during indentation. This disrupts the initial crystallographic order of the monolayers. In addition, a small number of hydrocarbon chains become pinned between the nanotube and the diamond substrate and cause a reordering of the monolayers. It has been suggested that related phenomena can occur in AFM experiments. Salmeron and co-workers observed a pressure-dependent structural transition in alkanethiols on Au.[7] This structural transition is thought to arise from the reversible lateral displacement of molecules from beneath the AFM tip. The thiol molecules are thought to remain in contact with the tip. This effect was only observed for sharp tips (tip radius ≈700−1000 Å.) It should be noted that the radius of the tips used in typical AFM experiments that have examined adhesion and friction of organic films,[15,42] alkylthiols on Au,[6,7] and alkylsilanes on mica and silicon[11,14] is typically on the order of hundreds of angstroms. The [10,10] single-wall nanotube used in the simulations discussed here is ~14 Å wide. Therefore, it is likely that a larger number of chains within the films would be pinned by the tip in an AFM experiment, perhaps forming a cushion for the tip.

Scanning alkylsilane films with AFM has been shown to cause irreversible damage.[9,51] This damage is attributed to a disruption of the cross-linked siloxane network. Simulations reported here also show that it is possible to initiate irreversible chemical changes within monolayers via indentation. In the sample simulations shown here, a carbon−carbon bond within a chain pinned by the tip is severed. This is the first reported instance of a simulated indentation-induced bond rupture in a monolayer system. Chain rupture has also been observed in subsequent simulations that have examined the friction of hydrocarbon monolayers.[37]

Salmeron and co-workers have suggested that indentation of alkanethiols and alkylsilanes using AFM can lead to the formation of gauche defects within the monolayers.[9] The nature of molecular dynamics simulations allows for the quantification of the number of defects formed and the determination of their exact location. Our simulations show that gauche defects are indeed formed as a result of the indentation process and these defects are localized to the region below and surrounding the nanotube tip. In addition, due to the small contact area of the nanotube used in the simulations, the number of defects formed is a function of penetration depth into the monolayer and is independent of the length of the monolayer chain. The number of defects present in the monolayers is important in light of recent quartz crystal microbalance experiments on C_9 alkanethiols on Au that suggest that the number of defects present in these monolayers affects energy dissipation within the films, thus affecting the measured friction.[52] The simulations also show that the indentation speed has a dramatic effect on the number of gauche defects formed. The origin of this behavior is not fully understood. It appears to be linked to both the time the tip is in contact with the monolayer and the geometry of the tip. Because the computational indentation speeds are orders of magnitude faster than speeds used in AFM experiments, it is difficult to ascertain whether this effect is present in AFM experiments. One can perhaps infer that quantitative AFM

measurements of friction on SAMs should be performed with all experimental parameters, even approach speed, being equal to those from previous studies.

It should be noted that the trends in elastic response of the hydrocarbon monolayers with chain length calculated in this work conflict with the trends in moduli inferred from AFM pull-off measurements. However, there are fundamental differences between these simulations and the experiments. The foremost difference is the uncertainty in the packing and structure of the alkanethiols on Au. In the simulations, there is one domain with identical packing for the C_8, C_{13}, and C_{22} monolayers and the monolayers are free of defects. Thus, any difference in elastic response arises solely from differences in the chain length. Experimentally, the packing of the short chain alkanethiols, less than 8 carbon atoms, does not appear to be the same as the longer chain molecules.[6,12,13,50] This difference has not been accounted for here. In addition, scanning tunneling microscopy experiments on alkanethiols on single-crystal Au(111) show that there can be multiple domains with incommensurate boundaries and inclusions of disordered molecules in regions as small as ~100 nm^2.[46] This is of the same magnitude as typical AFM contact areas and could easily affect measurements of the film's mechanical properties. The greater degree of disorder has been used to rationalize the softer modulus in short chains. It is worth noting that, while the shorter chains are indeed disordered in the current study, this alone is not enough to guarantee a smaller bulk modulus. More work must be done to determine the reason for this discrepancy. Future simulations will investigate how the disorder, packing differences, and domains experimentally found in these monolayers affect the elastic response of the monolayers.

References and Notes

(1) Tsukruk, V. V.; Nguyen, T.; Lemieux, M.; Hazel, J.; Weber, W. H.; Shevchenlco, V. V.; Klimenko, N.; Shelndko, E. Tribological Properties of Modified MEMS Surfaces. *Tribology Issues and Opportunities in MEMS*; Kluwer Academic Publishers: Dordrecht, Boston, London, 1998; pp 607−614.

(2) Deng, K.; Collins, R. J.; Mehregany, M.; Sukenik, C. N. *J. Electrochem. Soc.* **1995**, *142*, 1278.

(3) Homola, A. M.; Mate, C. M.; Street, G. B. *MRS Bull.* **1990**, *15*, 45−52.

(4) Perry, S. S.; Somorjai, G. A.; Mate, C. M.; White, R. L. *Tribol. Lett.* **1995**, *1*, 233−246.

(5) Perry, S. S.; Somorjai, G. A.; Mate, C. M.; White, R. *Tribol. Lett.* **1995**, *1*, 47−58.

(6) Lio, A.; Charych, D. H.; Salmeron, M. *J. Phys. Chem. B* **1997**, *101*, 3800−3805.

(7) Lio, A.; Morant, C.; Ogletree, D.; Salmeron, M. *J. Phys. Chem. B* **1997**, *101*, 4767−4773.

(8) Kim, H. I.; Graupe, M.; Oloba, O.; Doini, T.; Imaduddin, S.; Lee, T. R.; Perry, S. S. *Langmuir* **1999**, *15*, 3179−3185.

(9) Carpick, R. W.; Salmeron, M. *Chem. Rev.* **1997**, *97*, 1163−1194, and references therein.

(10) Kim, H. I.; Koini, T.; Lee, T. R.; Perry, S. S. *Langmuir* **1997**, *13*, 7192−7196.

(11) Xiao, X.; Hu, J.; Charych, D. H.; Salmeron, M. *Langmuir* **1996**, *12*, 235−237.

(12) Fenter, P.; Eisenberger, P.; Liang, K. S. *Phys. Rev. Lett.* **1993**, *70*, 2447−2450.

(13) Fenter, P.; Eberhardt, A.; Eisenberger, P. *Science (Washington, D.C.)* **1994**, *266*, 1216−1218.

(14) Harrison, J. A.; Perry, S. S. *MRS Bull.* **1998**, *23*, 27−31.

Indentation of Linear-Chain Hydrocarbon Monolayers

J. Phys. Chem. B, Vol. 103, No. 51, 1999 **11365**

(15) Koleske, D. D.; Barger, W. R.; Lee, G. U.; Colton, R. J. *Mater. Res. Soc. Symp. Proc.* **1997**, *464*, 377−383.

(16) Mar, W.; Klein, M. L. *Langmuir* **1994**, *10*, 188−196.

(17) Bhatia, R.; Garrison, B. J. *Langmuir* **1997**, *13*, 765−769.

(18) Bhatia, R.; Garrison, B. J. *Langmuir* **1997**, *13*, 4038−4043.

(19) Luedtke, W. D.; Landman, U. *J. Phys. Chem. B* **1998**, *102*, 6566−6572.

(20) Tupper, K. J.; Colton, R. J.; Brenner, D. W. *Langmuir* **1994**, *10*, 2041−2043.

(21) Tupper, K. J.; Brenner, D. W. *Langmuir* **1994**, *10*, 2335−2338.

(22) Tutein, A. B.; Stuart, S. J.; Harrison, J. A. *Langmuir*, in press.

(23) Dai, H.; Hafner, J. H.; Rinzler, A. G.; Colbert, D. T.; Smalley, R. *Nature (London)* **1996**, *384*, 147.

(24) Harrison, J. A.; Stuart, S. J.; Robertson, D. H.; White, C. T. *J. Phys. Chem. B* **1997**, *101*, 9682−9685.

(25) Yakobson, B.; Brabec, C.; Bernholc, J. *Phys. Rev. Lett.* **1996**, *76*, 2511−2514.

(26) Robertson, D.; Brenner, D.; Mintmire, *J. Phys. Rev. B: Condens. Matter* **1992**, *45*, 12592−12595.

(27) Garg, A.; Han, J.; Sinnott, S. B. *Phys. Rev. Lett.* **1998**, *81*, 2260−2263.

(28) Adelman, S. A.; Doll, J. D. *J. Chem. Phys.* **1976**, *64*, 2375−2388.

(29) Swope, W. C.; Andersen, H. C.; Berens, P. H.; Wilson, K. R. *J. Chem. Phys.* **1982**, *76*, 637−649.

(30) Stuart, S. J.; Tutein, A. B.; Harrison, J. A. *J. Chem. Phys.*, submitted 1999.

(31) Brenner, D. W. *Phys. Rev. B: Condens. Matter* **1990**, *42*, 9458−9471.

(32) Brenner, D. W.; Harrison, J. A.; Colton, R. J.; White, C. T. *Thin Solid Films* **1991**, *206*, 220−223.

(33) Garrison, B. J.; Dawnkaski, E. J.; Srivastava, D.; Brenner, D. W. *Science* **1992**, *255*, 835−838.

(34) Harrison, J. A.; Brenner, D. W. *J. Am. Chem. Soc.* **1994**, *116*, 10399−10402.

(35) Harrison, J. A.; Stuart, S. J.; Perry, M. D. The Tribology of Hydrocarbon Surfaces Investigated using Molecular Dynamics. *Tribol.*

(36) Harrison, J. A.; Tutein, A. B.; Stuart, S. J.; Robertson, D. H.; White, C. T., in preparation.

(37) Tutein, A. B.; Stuart, S. J.; Harrison, J. A. *Proceedings of the 218th ACS meeting symposium on Interfacial Properties on The Submicron Scale*, in press.

(38) Dubois, L. H.; Zegarski, B. R.; Nuzzo, R. G. *J. Chem. Phys.* **1993**, *98*, 678−688.

(39) Berman, A.; Israelachvilli, J. N. Surface Forces and Microrheology of Molecularly Thin Films. *CRC Handbook of Micro/Nanotribology*, 2nd ed., Bhushan, B. Ed.; CRC Press: Boca Raton, FL, 1999; pp 371−432.

(40) Hoffmann, H.; Mayer, U.; Krischanitz, A. *Langmuir* **1995**, *11*, 1304.

(41) Pharr, G. M.; Oliver, W. C.; Brotzen, F. R. *J. Mater. Res.* **1992**, *7*, 613−617.

(42) Overney, R. M.; Meyer, E.; Frommer, J.; Guntherodt, H.-J. *Langmuir* **1994**, *10*, 1281−1286.

(43) Zhdanov, G. S. *Crystal Physics*; Oliver and Boyd: Edinburgh and London, 1965; Chapter 16, pp 432−460.

(44) Winterstein, D. F. *Geophysics* **1990**, *55*, 1070−1088.

(45) Burns, A. R.; Houston, J. E.; Carpick, R. W.; Michalske, T. A. *Phys. Rev. Lett.* **1999**, *82*, 1181−1184.

(46) Poirier, G. E.; Tarlov, M. J.; Rushmeirer, H. E. *Langmuir* **1994**, *10*, 3383.

(47) Treacy, M.; Ebbesen, T.; Gibson, J. *Nature (London)* **1996**, *381*, 678−680.

(48) Cornwell, C. F.; Wille, L. T. *Solid State Commun.* **1997**, *101*, 555−558.

(49) Tersoff, J.; Ruoff, R. S. *Phys. Rev. Lett.* **1994**, *73*, 676−679.

(50) Camillone, N.; Chidsey, C. E. D.; Liu, G.-Y.; Scoles, G. J. *J. Chem. Phys.* **1991**, *94*, 8493−8502.

(51) Xiao, X.; Lui, G.-Y.; Charych, D. H.; Salmeron, M. *Langmuir* **1995**, *11*, 1600−1604.

(52) Shinn, N. D.; Mayer, T. M.; Michalske, T. A. *Tribol. Lett.*, in press.

Issues and Opportunities in MEMS; Kluwer Academic Publishers: Dordrecht, Boston, London, 1998; pp 285−299.